Sensors & Transducers, Vol. 235, Issue 7, July 2019, pp. 1-8

Sensors & Transducers

Published by IFSA Publishing, S. L., 2019
http://www.sensorsportal.com

Theoretical Consideration on Potential and Scalability of Optical Rotors based on a pn-Junction Rod

Yasuhisa OMURA

Kansai University, 3-3-35 Yamate-cho, Suita, 564-8680, Japan
ACA & C, Okazaki, Isehara, 259-1135, Japan
Tel.: +81-6-6368-1121, fax: +81-6-6368-8843
E-mail: omuray@kansai-u.ac.jp

Received: 15 April 2019 /Accepted: 28 May 2019 /Published: 31 July 2019

Abstract: This paper theoretically investigates how a Si pn-junction rod offers the potential to develop rotating motion. An analytical steady state solution of excess carrier concentration of the Si rod is derived from the continuity equation. The solution is given by a non-linear differential equation. Numerical calculation results strongly suggested that a 200-µm-long Si rod should rotate with the acceleration of ~10^3 m/s^2 under the illumination of 1 W/cm^2. This is very good performance. It is also shown that this performance holds even for nano-scale rod rotors. It is expected that such rotors will suit various medical test chips that have no battery.

Keywords: pn junction, Rod, Light illumination, Rotation, Carrier generation, Recombination, Power generation.

1. Introduction

Micro Electro Mechanical System (MEMS) technology was proposed in the last century [1-2], and its fundamental potentiality has been technically and commercially examined in various applications [3-5]. Given the old-fashioned technology available at its introduction, it was simply expected that MEMS device scale would range from hundreds of micrometers to few micrometers. However, this simple expectation has been proven flawed in real applications because achieving adequate reproducibility in device fabrication demanded very fine processing techniques, resulting high production costs. These technical barriers are missing in the "Nano-imprint technique" [6] and "3D printer technique" [7-8]; they were proposed in the 1980s and 1990s, respectively, as advances from the original MEMS technology. Their advancement continues as well-known technologies.

Unfortunately, the demands imposed on MEMS devices in the health control and medical care fields are becoming more urgent in various communities all over the world. The MEMS devices created to meet requests [9-11], must have better low-power operation because most of them must work with very small batteries, not with ac power supplies. In extreme cases, cord-free operation is required. Such devices need a built-in battery that is charged by an external energy source. Although I proposed the advanced Schenkel circuit for RF-ID applications [12], the idea remains to be confirmed in practical applications.

Recently, the author proposed an optical rotor based on a pn-junction rod [13], and theoretically predicted its performance [14].

In this paper, the author theoretically examines the performance of the optical rotor in detail. It should work when irradiated by green light. The fundamental function and operation of the device are formulated mathematically based on semiconductor physics. In addition, its technological potential and scalability are also addressed.

2. Possible Device Structure and Rotation Principle

2.1. Possible Device Structure

The Si-based pn-junction rod discussed here is shown in Fig. 1. It is assumed to have length of $2L$, width of W, and height of H. H is the silicon layer thickness (t_s). The doping level of the p-type region is N_A and that of the n-type region is N_D. The light comes illuminates the upper side of the rod with power of P_{ph} (W/cm^2). It is assumed to be monochromatic light with wavelength of λ; here green light is assumed.

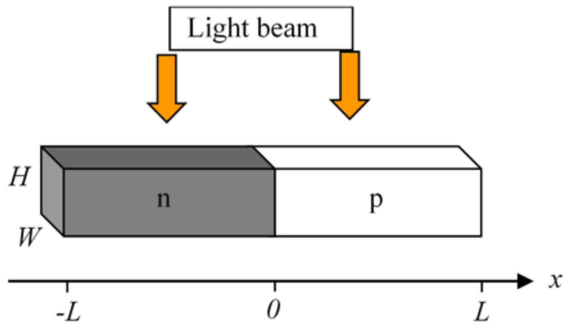

Fig. 1. pn junction rod.

When N_{ph} photons per unit area and per unit time arrive at the surface of the rod, we have

$$P_{ph} = N_{ph} h \frac{c}{\lambda}. \quad (1)$$

The photon energy should be larger than the bandgap energy of the semiconductor material. The resulting generation rates of electrons and holes (G_n and G_p in units of s^{-1}cm^{-3}) are expressed as

$$G_n = \frac{N_{ph}}{t_s}(1-R)l_C\left[1-\exp\left(-\frac{t_S}{l_C}\right)\right], \quad (2)$$

$$G_p = \frac{N_{ph}}{t_s}(1-R)l_C\left[1-\exp\left(-\frac{t_S}{l_C}\right)\right], \quad (3)$$

where R is the reflectance and l_c is the absorption length.

2.2. Rotation Principle

A schematic view of the rotor is shown in Fig. 2, where the pn-junction rotor is located at the center of the cavity space. It is assumed that the distance from the center of the rotor to the external electrode is D. When the light beam irradiates the surface of the pn-junction rod, electron-hole generation occurs in both the p-type and the n-type region. The p-type region is charged positively and the n-type region negatively.

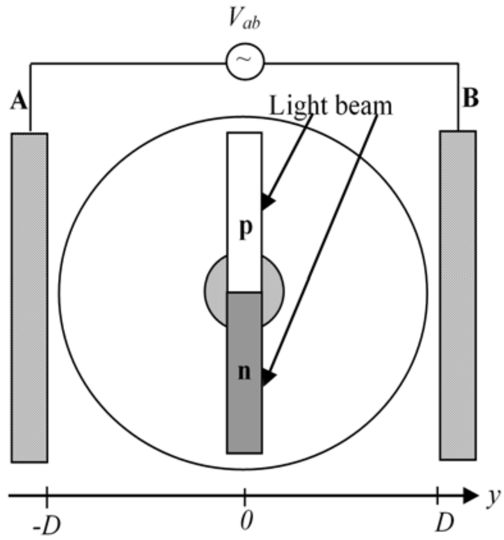

Fig. 2. Rotation mechanism. A and B denote the electrodes.

When the external electrodes, A and B, are alternatively biased, the rod will continue to rotate as long as the rod is irradiated. In order to ensure stable rotation of the rod, the frequency of the ac voltage must match the rotation period.

3. Theoretical Base of Rod Rotation

3.1. Carrier Generation and Recombination under the Light Illumination

The electron generation and recombination process in the p-type region generally follows the differential equation shown below.

$$\frac{\partial n_p(x,t)}{\partial t} = G_n - \frac{n_p(x,t) - n_{p0}}{\tau_n} + n_p \mu_n \frac{\partial F}{\partial x} + \mu_n F \frac{\partial n_p}{\partial x} + D_n \frac{\partial^2 n_p}{\partial x^2}, \quad (4)$$

where n_{p0} denotes the electron concentration at thermal equilibrium, G_n denotes the generation rate of electrons, τ_n denotes the lifetime of electrons, F denotes the local electric field, μ_n denotes the electron mobility, and D_n denotes the diffusion constant of electrons.

The hole generation and recombination process in the n-type region generally follows the differential equation shown below.

$$\frac{\partial p_n(x,t)}{\partial t} = G_p - \frac{p_n(x,t) - p_{n0}}{\tau_p} - p_n \mu_p \frac{\partial F}{\partial x} - \mu_p F \frac{\partial p_n}{\partial x} + D_p \frac{\partial^2 p_n}{\partial x^2}, \quad (5)$$

where p_{n0} denotes the hole concentration at thermal equilibrium, G_p denotes the generation rate of holes, τ_p denotes the lifetime of holes, μ_p denotes hole mobility, and D_p denotes the diffusion constant of holes. Holes generated in the n-type region flow toward the p-type region. In the p-type region, the whole holes including those coming from the n-type region must follow the following continuity equation.

$$\frac{\partial p_p(x,t)}{\partial t} = G_p - \frac{p_p(x,t) - p_{p0}}{\tau_p} - p_p \mu_p \frac{\partial F}{\partial x} - \mu_p F \frac{\partial p_p}{\partial x} + D_p \frac{\partial^2 p_p}{\partial x^2} \quad (6)$$

The local electric field follows Poisson's equations as shown below.

$$-\frac{\partial F}{\partial x} = -\frac{e}{\varepsilon_S}(p_p - p_{po} - n_p + n_{p0}), \quad (7)$$

$$-\frac{\partial F}{\partial x} = -\frac{e}{\varepsilon_S}(p_n - p_{n0} - n_n + n_{n0}), \quad (8)$$

where e is the magnitude of the elementary charge, and ε_s is the semiconductor's permittivity.

3.2. Steady State Solutions

At the steady state, we have

$$G_n - \frac{n_p(x,t) - n_{p0}}{\tau_n} + n_p \mu_n \frac{\partial F}{\partial x} + \mu_n F \frac{\partial n_p}{\partial x} + D_n \frac{\partial^2 n_p}{\partial x^2} = 0, \quad (9)$$

$$G_p - \frac{p_n(x,t) - p_{n0}}{\tau_p} - p_n \mu_p \frac{\partial F}{\partial x} - \mu_p F \frac{\partial p_n}{\partial x} + D_p \frac{\partial^2 p_n}{\partial x^2} = 0, \quad (10)$$

$$G_p - \frac{p_p(x,t) - p_{p0}}{\tau_p} - p_p \mu_p \frac{\partial F}{\partial x} - \mu_p F \frac{\partial p_p}{\partial x} + D_p \frac{\partial^2 p_p}{\partial x^2} = 0 \quad (11)$$

Poisson's Eq. (7) and Eq. (8) can be approximately rewritten as

$$-\frac{\partial F}{\partial x} \cong -\frac{e}{\varepsilon_S}(p_p - N_A), \quad (12)$$

$$-\frac{\partial F}{\partial x} \cong -\frac{e}{\varepsilon_S}(-n_n + N_D) \quad (13)$$

These approximations are allowed based on charge neutrality in the system. Eq. (12) means that the hole concentration in the p-type region is ruled by the sum of the holes generated in the p-type region and those coming from the n-type region. Eq. (13) also means the physical phenomenon for electrons is similar to that of holes in the p-type region.

First we calculate the steady state hole concentration in the p-type region using Eq. (12). When Eq. (12) is integrated, we assume the local gradient of (p_p - N_A) is not so large. Hence, we have

$$F \cong \frac{e}{\varepsilon_S}(p_p - N_A) L_{Dp}, \quad (14)$$

where L_{Dp} is the Debye length in the p-type region. Eq. (11) is rewritten as

$$D_p \frac{\partial^2 p_p}{\partial x^2} - \left(\frac{eL_{Dp}\mu_p}{\varepsilon_S}\right)\left(2p_p \frac{\partial p_p}{\partial x} - N_A \frac{\partial p_p}{\partial x}\right) - \frac{p_p(x,t) - N_A - G_p\tau_p}{\tau_p} = 0 \quad (15)$$

We replace the expression for $p_p(x)$ with the following function $P(x)$, which represents the excess hole concentration.

$$P(x) = p_p(x) - N_A - G_p\tau_p \quad (16)$$

The above yields

$$\frac{\partial^2 P}{\partial x^2} - A_p P \frac{\partial P}{\partial x} - B_p \frac{\partial P}{\partial x} - C_P P = 0, \quad (17)$$

$$A_P = \frac{2eL_{Dp}\mu_p}{D_p \varepsilon_S}, \quad (18)$$

$$B_P = \left(\frac{eL_{Dp}\mu_p}{D_p \varepsilon_S}\right)(N_A + 2G_p\tau_p), \quad (19)$$

$$C_P = \frac{1}{D_p \tau_p} \quad (20)$$

Eq. (17) can be approximately solved for two cases. Thus we have the following solution for $P(x)$. See Appendix A.

$$P(x)=\frac{2\frac{\sqrt{2C_P}}{A_P}\frac{P(0)}{P(0)+2\frac{\sqrt{2C_P}}{A_P}}\exp\left(\sqrt{2C_p}x\right)}{1-\frac{P(0)}{P(0)+2\frac{\sqrt{2C_P}}{A_P}}\exp\left(\sqrt{2C_p}x\right)} \tag{21}$$

We have the following solution for the excess electron density profile N(x) in the n-type region by using a similar calculation.

$$N(x)=\frac{2\frac{\sqrt{2C_n}}{A_n}\frac{N(0)}{N(0)+2\frac{\sqrt{2C_n}}{A_n}}\exp\left(\sqrt{2C_n}x\right)}{1-\frac{N(0)}{N(0)+2\frac{\sqrt{2C_n}}{A_n}}\exp\left(\sqrt{2C_n}x\right)}, \tag{22}$$

where

$$N(0)=n_n(0)-N_D-G_n\tau_n, \tag{23}$$

$$A_n=\frac{2eL_{Dn}\mu_n}{D_n\varepsilon_S}, \tag{24}$$

$$C_n=\frac{1}{D_n\tau_n} \tag{25}$$

This expression for the excess electron density exhibits complementary behavior against the excess hole density as is shown in the following section. Excess electron density in the p-type region and excess hole density in the n-type region can't be analytically derived from the continuity equation because of its strong non-linearity. It should be solved numerically if necessary.

3.3. Force of Rotation

Coordinates to calculate the rotation torque are shown in Fig. 3. In this system, for simplicity, we assume that the potential difference of the two electrodes is constant (V_{abm}) for $-\pi< \theta <0$. The local force $F_\theta(r)$ on the rod is given by

$$dF_\theta(r)=-\frac{Mr}{2L}\left(\frac{d^2\theta}{dt^2}\right)dr, \tag{26}$$

where M is the mass of the rod. An approximate expression of the force is given by (see Appendix B)

$$F_\theta(L,t)=\frac{eWHV_{ab}(t)\sin\theta}{2D}\times\left[\int_0^L P(r)dr+G_p\tau_pL\right] \tag{27}$$

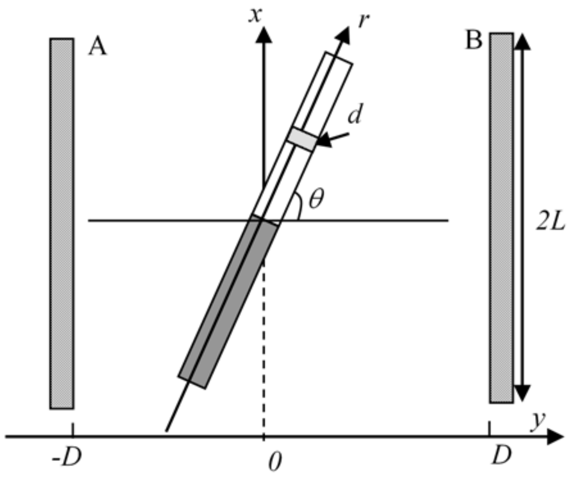

Fig. 3. Force to induce the rotation of the rod.

4. Simulation Results and Discussion

4.1. Large Devices

Here the calculation results of some key parameters are shown. It has been numerically verified that the assumption of a linear approximation does not result in an appropriate solution. This section, therefore, adopts a non-linear differential equation for the numerical calculations. Calculation results of excess hole distribution in the p-type region of the rod are shown in Figs. 4, 5, 6 and 7, where device parameters are listed in Table 1 and green-light illumination is assumed.

Table 1. Control Device Parameters and Material Parameters Assumed.

Parameters	Values [units]	
	Large Devices	Small Devices
L	100 [μm]	1 [μm]
Y	0.1~2 [μm]	10 [nm]
W	1 [μm]	100 [nm]
D	125 [μm]	1.5 [μm]
N_A, N_D	10^{15}~10^{17} [cm^{-3}]	
τ_n, τ_p	0.01~1.0 [μs]	
l_c	0.55 [μm]	
V_{ab}	1 [V]	

All simulations for the large devices indicated that a rod length of tens of microns was most suitable. Fig. 4 plots the excess hole concentration versus distance from the rod center for three illumination power values (P_{ph}, units of W/cm^2). Fig. 5 plots the same curves but three rod thickness values (H, units of microns). Fig. 6 plots the same curves for three doping concentration values (N_A, N_D, units of cm^{-3}), and Fig. 7 shows the same curves for three carrier lifetime values (τ_n, τ_p, units of μs).

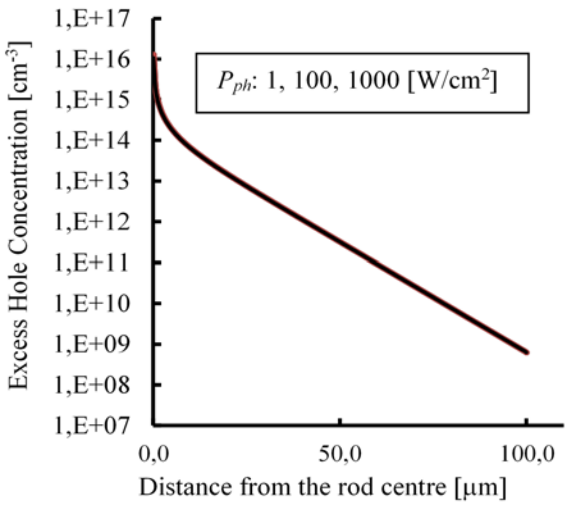

Fig. 4. Excess hole concentration with parameter of illumination power.

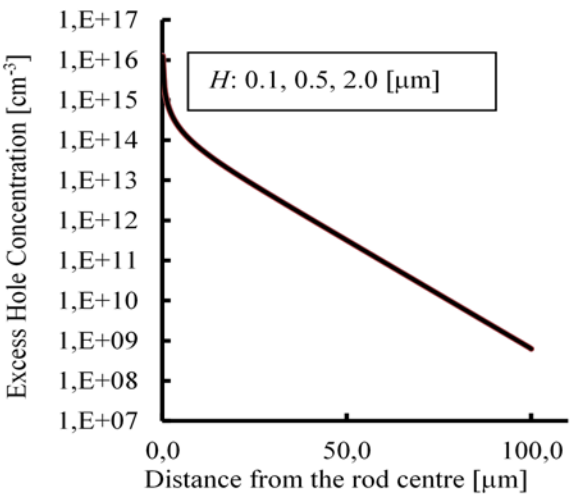

Fig. 5. Excess hole concentration with parameter of rod thickness.

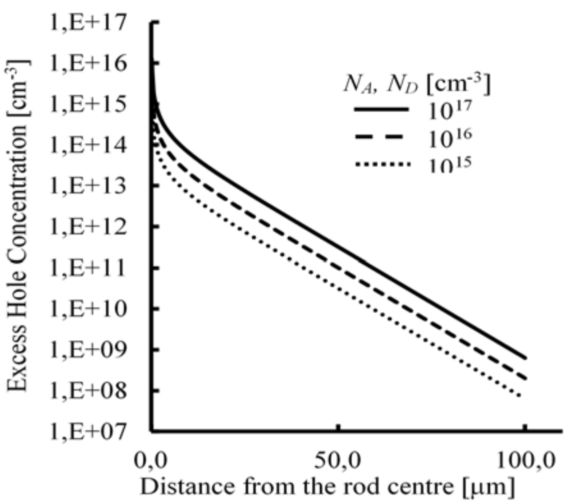

Fig. 6. Excess hole concentration with parameter of doping concentration.

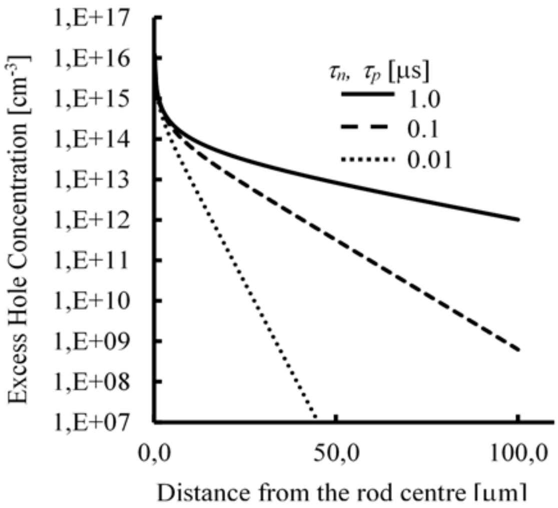

Fig. 7. Excess hole concentration with parameter of carrier lifetime.

Fig. 4 reveals that excess hole concentration is not sensitive to the illumination, with is counter to the expectation. This suggests that very low power operation is available. Fig. 5 reveals that excess hole concentration is not sensitive to rod thickness, which suggests that carrier generation is not sensitive to local variations in rod thickness. Fig. 6 reveals that the excess hole concentration increases with the doping concentration, which suggests that care is needed in designing the doping concentration. Fig. 7 shows that the excess hole concentration profile is very sensitive to carrier lifetime as expected. Since poly-Si film is usually assumed, we must consider the crystallinity of the film. All these results reinforce the high potential for Si rod rotation under low-power light illumination.

We also calculated the force of rod rotation using Eq. (27). When we assume the parameter values shown in Table 1, the rotation force is about 10^{-9} N. Since the mass of the Si rod is about 9.2×10^{-13} kg, its acceleration is about 10^3 m/s^2. Since this value is very large, it is expected that the Si rod will rotate rapidly even under weak illumination.

4.2. Small Devices

Here calculation results of excess hole distribution in the p-type region of the scaled rod are shown in Figs. 8, 9 and 10, where green-light illumination is assumed. Devices parameters assumed are listed in Table 1. In nano-scale devices, the photon energy should be larger than the effective bandgap energy (E_G*) of the semiconductor material; the effective bandgap energy is larger than the intrinsic bandgap energy (E_G) [15] because of the physical confinement.

Fig. 8 reveals that excess hole concentration near the rotor center is sensitive to the illumination power because most holes come from the n-type region; this behavior was not seen in a large scale rotor [14].

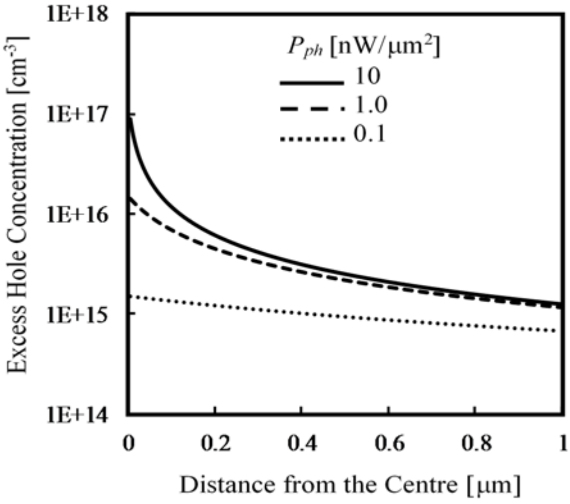

Fig. 8. Excess hole concentration with parameter of illumination power of green light.

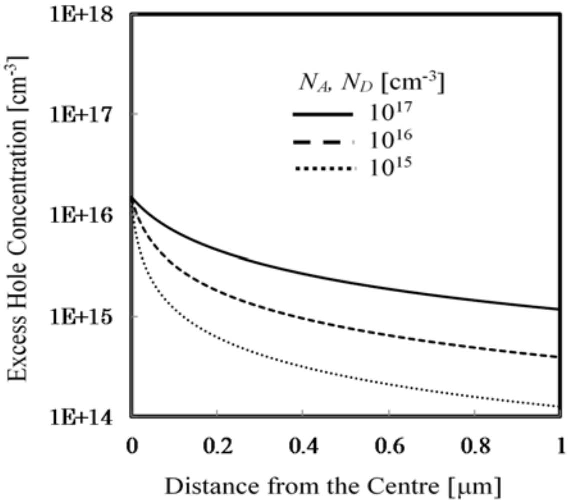

Fig. 9. Excess hole concentration with parameter of doping concentration.

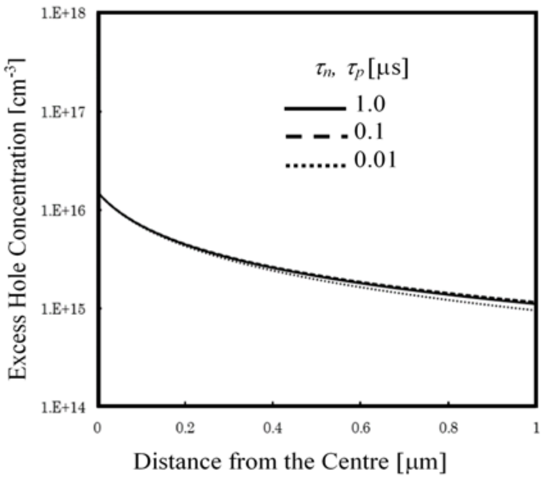

Fig. 10. Excess hole concentration with parameter of carrier lifetime.

Fig. 9 reveals that the excess hole concentration definitely increases with the doping concentration, which suggests that care is needed in designing the doping concentration.

Fig. 10 shows that the excess hole concentration profile is almost insensitive to carrier lifetime in contrast to the large scale rotor [14].

This is a great merit of nano-scale rotor because a poly-Si film has a very short lifetime. It is not necessary to worry about the material quality. All these results reinforce the high potential for nano-scale Si pn-junction wire rotation under low-power light illumination.

The force of rod rotation was calculated using Eq. (27) [14]. When we assume that V_{ab} = 1 V, H = 10 nm, $\tau_n=\tau_p$ = 1 µs, $N_A=N_D$ = 10^{17} cm^{-3}, and the distance of electrode (2D) is 3 µm, the rotation force is about 2.6×10^{-13} N. Since the mass of the Si rod is about 2.3×10^{-15} kg, its acceleration is about 10^2 m/s^2. Since this value is very large, it is expected that the Si wire will rotate rapidly even under weak illumination.

It is expected that the device reveals very good performance. Thus, this device is applicable as a mixer of chemical solutions in various robots for medical diagnostics without any internal battery.

5. Conclusions

This paper introduced a theoretical model and numerical simulations to investigate the potential and scalability of using a Si pn-junction rod as a mechanical rotor. An analytical, but approximated, steady state solution of excess carrier concentration of the Si rod was derived from the non-linear continuity equation. Simulation results strongly suggested that a 200-µm-long Si rod should rotate with the acceleration of ~10^3 m/s^2 under the illumination of 1 W/cm^2.

In addition, when we assume that V_{ab} = 1 V, H = 10 nm, $\tau_n=\tau_p$ = 1 µs, $N_A=N_D$ = 10^{17} cm^{-3}, and the distance of electrode (2D) is 3 µm, the rotation force is about 2.6×10^{-13} N. Since the mass of the Si rod is about 2.3×10^{-15} kg, its acceleration is about 10^2 m/s^2.

Since the above values of acceleration are very large, it is expected that the Si wire will rotate rapidly even under weak illumination. This is very good performance. Thus, this device is applicable as a mixer of chemical solutions in various medical test chips and medical robots that have no battery.

Acknowledgements

A part of this study was financially supported by “Strategic Project to Support the Formation of Research Bases at Private Universities” in Japan: Matching Fund Subsidy from MEXT (Ministry of Education, Culture, Sports, Sciences and Technology), 2015-2019, in Japan.

References

[1]. Nathanson H. C., Newell W. E., Wickstrom R. A., Davis J. R., The resonant gate transistor, *IEEE Trans. Electron Devices*, Vol. 14, Issue 3, 1967, pp. 117-133.

[2]. E. J. Garcia, J. J. Sniegowski, Surface Micromachined Microengine, *Sensors and Actuators A*, Vol. 48, Issue 3, 1995, pp. 203-214.

[3]. G. Piazza, V. Felmetsger, P. Muralt, R. H. Olsson III, R. Ruby, Piezoelectric Aluminum Nitride Films for Microelectromechanical Systems, MRS Bulletin, Vol. 37, Issue 11, 2012, pp. 1051-1061.

[4]. X. Yan, M. Qi, L. Lin, Self-lifting Artificial Insect Wings via Electrostatic Flapping actuators, in *Proceedings of the 28th IEEE Int. Conf. on MEMS,* Estoril, Portugal, Jan. 2015, pp. 22-25.

[5]. D. Kang, K. Murali, N. Scianmarello, J. Park, J. H.-C. Chang, Y. Liu, K.-T. Chang, Y.-C. Tai, M. S. Humayun, MEMS Oxygen Transporter to Treat Retinal Ischemia, in *Proceedings of the 28th IEEE Int. Conf. on MEMS,* Estoril, Portugal, Jan, 2015, pp. 154-157.

[6]. S. Y. Chou, P. R. Krauss, P. J. Renstrom, Nanoimprint Lithography, *J. Vac. Sci. & Technol. B*, Vol. 14, Issue 6, 1996, pp. 4129-4133.

[7]. H. Kodama, Invention of Photo-Solidilying Modeling Method, *Macro Rev.*, Vol. 9, Issue 2, 1997, pp. 59-79.

[8]. A. J. Herbert, Solid Object Generation, *J. Appl. Photographic Eng.*, Vol. 8, Issue 4, 1982, pp. 185-188.

[9]. N. Inomata, Y. Yamanishi, F. Arai, Manipulation and Observation of Carbon Nanotubes in Water Under an Optical Microscope Using a Microfluidic Chip, *IEEE Trans. Nanotechnol*., Vol. 8, Issue 4, 2009, pp. 463-468.

[10]. C. M. Puleo, H. C. Yeh, T. H. Wang, Applications of MEMS Technologies in Tissue Engineering, *Tissue Eng*., Vol. 13, Issue 12, 2007, pp. 2839-2854.

[11]. M. Noda, P. Lorchirachoonkul, T. Shimanouchi, K. Yamashita, H. Umakoshi, R. Kuboi, Sensitivity Enhancement of Leakage Current Microsensor for Detection of Target Protein by Using Protein Denaturant, *IEEE Sensors J.*, Vol. 11, Issue 11, 2011, pp. 2749-2755.

[12]. Y. Omura, Y. Iida, Performance Prospects of Fully-Depleted SOI MOSFET-Based Diodes Applied to Schenkel Circuit for RF-ID Chips, *Sci. Res., J. Cir. and Syst.*, Vol. 4, Issue 2, 2013, pp. 173-180.

[13]. Y. Omura, Rotor, Jpn. Pat. No. 6470993, 2019.

[14]. Y. Omura, Theoretical Consideration of an Optical Rotor Using a Si pn-Junction Rod, in *Proceedings of the 2nd International Conference on Microelectronic Devices and Technologies (MicDAT '2019),* Amsterdam, The Netherlands, 2019, pp. 11-15.

[15]. Y. Omura, Two-Dimensionally Confined Injection Phenomena at Low Temperatures in Sub-10-nm-Thick SOI Insulated-Gate p-n-Junction Devices, *IEEE Trans. Electron Devices*, Vol. 43, Issue 3, 1996, pp. 436-443.

Appendix A: Solution of Eq. (17)

When the number of carriers generated is high, the nonlinear term of Eq. (17) can't be discarded.

$$\frac{\partial^2 P}{\partial x^2} - A_p P \frac{\partial P}{\partial x} - C_P P = 0 \tag{A1}$$

By multiplying $\frac{\partial P}{\partial x}$ to both side, we can integrate the equation.

$$\frac{1}{2}\left(\frac{\partial P}{\partial x'}\right)^2\Bigg|_0^x - A_p \int_0^x P \frac{\partial P}{\partial x'}\frac{\partial P}{\partial x'} dx' - C_P P^2\Big|_0^x = 0 \tag{A2}$$

Since the second term of the left-hand side can't be calculated as it is, we partially integrate the term as shown below.

$$\int_0^x P \frac{\partial P}{\partial x'}\frac{\partial P}{\partial x'} dx' = \left[\frac{1}{2}P^2 \frac{\partial P}{\partial x'}\right]_0^x - \frac{1}{2}\int_0^x P^2 \frac{\partial^2 P}{\partial x'^2} dx' \tag{A3}$$

We replace $\frac{\partial^2 P}{\partial x^2}$ in Eq. (A3) with the other expression using Eq. (A2), where we apply the following approximate relationship by neglecting the last term of the left-hand side of Eq. (A1) because the nonlinear aspect of Eq. (17) must be taken into account.

$$\frac{\partial^2 P}{\partial x^2} - A_p P \frac{\partial P}{\partial x} \cong 0 \tag{A4}$$

As a result, we have

$$\int_0^x P \frac{\partial P}{\partial x'}\frac{\partial P}{\partial x'} dx' = \left[\frac{1}{2}P^2 \frac{\partial P}{\partial x'}\right]_0^x - \frac{A_P}{8} P^4\Big|_0^x \tag{A5}$$

Using Eq. (A5), we rewrite Eq. (A2) as

$$\left(\frac{\partial P}{\partial x}\right)^2 - A_P P^2 \frac{\partial P}{\partial x} + \frac{A_P^2}{4} P^4(x) - 2C_P P^2(x) + P_{00} = 0, \tag{A6}$$

where

$$P_{00} = -\left(\frac{\partial P}{\partial x}\right)^2_{x=0} + A_P P^2(0)\frac{\partial P}{\partial x}\bigg|_{x=0} - \frac{A_P^2}{4}P^4(0) + 2C_P P^2(0). \tag{A7}$$

We have the following equation from Eq. (A6).

$$\frac{dP}{dx} = \frac{1}{2}A_P P^2(x) \pm \sqrt{2C_P P^2(x) - P_{00}}, \tag{A8}$$

and then we can have the integration form of Eq. (A8).

$$\int \frac{dP}{P^2(x) \pm 2\frac{\sqrt{2C_P}}{A_P}\sqrt{P^2(x) - P_{00}/2C_P}} = \int \frac{A_P}{2} dx \tag{A9}$$

However, the above integration can't be performed analytically as it is. It is expected that $P_{00} << N_A$ because the primary part of P_{00} is the hole concentration around the metallurgical junction. Therefore we discard the term in Eq. (A9), which yields

$$\int \frac{dP}{P^2(x) \pm 2\frac{\sqrt{2C_P}}{A_P}\sqrt{P^2(x)}} = \int \frac{A_P}{2}dx, \tag{A10}$$

This integration is easily calculated as

$$\log\left(\frac{P(x)}{P(x) \pm 2\frac{\sqrt{2C_P}}{A_P}}\right) = \pm\sqrt{2C_P}\,x + P_{01}, \tag{A11}$$

$$P_{01} = \log\left(\frac{P(0)}{P(0) \pm 2\frac{\sqrt{2C_P}}{A_P}}\right). \tag{A12}$$

Thus we have the solution for $P(x)$ as shown by Eq. (21).

Appendix B: Force to Induce Rotation of Photon-irradiated pn-junction Rod

It is assumed that the time-dependent voltage $V_{ab}(t)$ is applied to the electrodes A and B. In Fig. 3, the excess hole charge ($dQ_p(r)$) in the small element with the length of dr in the n-type region is expressed as

$$dQ_p(r) = eWH\left[P(r) + G_p\tau_p\right]dr, \tag{B1}$$

where W and H are the width and the height of the cross-section of the rod. The force component (dF_θ) that establishes a rotation torque on the n-type region of the rod is expressed as

$$dF_\theta(r,t) = \frac{eWHV_{ab}(t)\sin\theta}{2D} \times\left[P(r) + G_p\tau_p\right]dr, \tag{B2}$$

Integration of Eq. (B2) yields the following rotation force.

$$F_\theta(L,t) = \frac{eWHV_{ab}(t)\sin\theta}{2D} \times\left[\int_0^L P(r)dr + G_p\tau_pL\right], \tag{B3}$$

On the other hand, Newton's equation is given by

$$dF_\theta(r) = -\frac{Mr}{2L}\left(\frac{d^2\theta}{dt^2}\right)dr, \tag{B4}$$

where M is the mass of the rod. Combining Eqs. (B2) and (B4) yields the following differential equation for the whole rod.

$$\left(\frac{d^2\theta}{dt^2}\right)rdr = -\frac{eWHLV_{ab}(t)\sin\theta}{MD} \times\left\{P(r) + G_p\tau_p + N(r) + G_n\tau_n\right\}dr, \tag{B5}$$

where this expression takes account of the excess charge in the p-type region. Integration of Eq. (B5) with coordinate r from 0 to L gives the following solution.

$$\left(\frac{d^2\theta}{dt^2}\right) = -\frac{2eWHV_{ab}(t)\sin\theta}{MD} \times\left\{G_p\tau_p + G_n\tau_n\right\} - \frac{2eWHV_{ab}(t)\sin\theta}{LMD}\left[\int_0^L (N(r)+P(r))dr\right]. \tag{B6}$$

This gives the averaged acceleration factor.